GA-A24497

EDGE RADIAL ELECTRIC FIELD STRUCTURE IN QUIESCENT H–MODE PLASMAS IN THE DIII–D TOKAMAK

by
K.H. BURRELL, W.P. WEST, E.J. DOYLE, M.E. AUSTIN,
J.S. deGRASSIE, P. GOHIL, C.M. GREENFIELD, R.J. GROEBNER,
R. JAYAKUMAR, D.H. KAPLAN, L.L. LAO, A.W. LEONARD,
M.A. MAKOWSKI, G.R. McKEE, W.M. SOLOMON, D.M. THOMAS,
T.L. RHODES, M.R. WADE, G. WANG, J.G. WATKINS, and L. ZENG

OCTOBER 2003

DISCLAIMER

GA-A24497

EDGE RADIAL ELECTRIC FIELD STRUCTURE IN QUIESCENT H–MODE PLASMAS IN THE DIII–D TOKAMAK

by
K.H. BURRELL, W.P. WEST, E.J. DOYLE,[£] M.E. AUSTIN,[§]
J.S. deGRASSIE, P. GOHIL, C.M. GREENFIELD, R.J. GROEBNER,
R. JAYAKUMAR,[¶] D.H. KAPLAN, L.L. LAO, A.W. LEONARD,
M.A. MAKOWSKI, [¶] G.R McKEE,[¥] W.M. SOLOMON,[†] D.M. THOMAS,
T.L. RHODES,[£] M.R.WADE, [°] G. WANG,[£] J.G. WATKINS,[‡]
and L. ZENG[£]

This is a preprint of a paper to be presented at the 9th IAEA Tech. Mtg on H-Mode Physics and Transport Barriers, San Diego, California, September 24-26, 2003, and to be printed in the *Proceedings*.

[£]University of California, Los Angeles, Los Angeles, CA
[§]University of Texas at Austin, Austin, TX
[¶]Lawrence Livermore National Laboratory, Livermore, CA
[¥]University of Wisconsin, Madison, WI
[†]Princeton Plasma Physics Laboratory, Princeton, NJ
[°]Oak Ridge National Laboratory, Oak Ridge, TN
[‡]Sandia National Laboratories, Albuquerque, NM

**Work supported by
the U.S. Department of Energy
under DE-AC03-99ER54463, W-7405-ENG-48,
DE-AC02-76CH03073, DE-AC05-00OR22725,
DE-AC04-94AL85000, DE-FG03-01ER54615,
DE-FG03-97ER54415, and DE-FG03-96ER54373**

**GENERAL ATOMICS PROJECT 30033
OCTOBER 2003**

ABSTRACT

H–mode operation is the choice for next step tokamak devices based either on conventional or advanced tokamak physics. This choice, however, comes at a significant cost for both the conventional and advanced tokamaks because of the effects of edge localized modes (ELMs). ELMs can produce significant erosion in the divertor and can affect the beta limit and reduced core transport regions needed for advanced tokamak operation. Experimental results from DIII–D over the past four years have demonstrated a new operating regime, the quiescent H–mode regime, which solves these problems. QH–mode plasmas have now been run for over 4 s (>30 energy confinement times). Utilizing the steady-state nature of the QH–mode edge allows us to obtain unprecedented spatial resolution of the edge ion profiles and the edge radial electric field E_r by slowly sweeping the edge plasma past the viewpoints of the charge exchange spectroscopy system. We have investigated the effects of direct edge ion orbit loss on the creation and sustainment of the QH–mode. Direct loss of ions injected into the velocity-space loss cone at the plasma edge is not necessary for creation or sustainment of the QH–mode. The direct ion orbit loss has little effect on the edge E_r well. The E_r at the bottom of the well in these cases is about –100 kV/m compared to –20 to –30 kV/m in standard H–mode. The well is about 1 cm wide, which is close to the diameter of the deuteron gyro-orbit. We also have investigated the effect of changing edge triangularity by changing the plasma shape from upwardly biased single null to magnetically balanced double null. We have now achieved QH–mode in these double-null plasmas. The increased triangularity allows us to increase pedestal density in QH–mode plasmas by a factor of about 2.5 and overall pedestal pressure by a factor of two. Pedestal beta and ν^* values matching the values desired for ITER have been achieved. In these higher density plasmas, the E_r well is significantly shallower and broader.

1. INTRODUCTION

The superior energy confinement time in H–mode makes it the preferred operating mode for next step tokamak devices utilizing either conventional [1] or advanced tokamak physics [2,3]. However, the effects of the associated edge localized modes (ELM) have a significant impact on machine design and operation. The pulsed divertor heat and particle loads due to standard, type I ELMs can lead to rapid erosion of the divertor plates [4–6]. In addition, for the advanced tokamak, type I ELMs can couple to core MHD modes (e.g., neoclassical tearing modes) and thus reduce the beta limit. Furthermore, type I ELMs can destroy the reduced transport core which is needed for the profile optimization required for advanced tokamak operation [7]. Accordingly, considerable effort is going into research to mitigate the effects of type I ELMs [4–6].

The conventional view is that ELMs are necessary for density and impurity control in H–mode. The standard, ELM-free H–mode typically exhibits monotonically increasing density and radiated power, which leads, ultimately, to radiative collapse. Experimental results in the last four years on the DIII–D tokamak have demonstrated a new type of H–mode operation which allows ELM-free operation at constant density and radiated power [9–18]. This quiescent H–mode (QH–mode) exhibits the H–mode confinement improvement without the detrimental effects of ELMs and without the problems exhibited by standard, ELM-free H–mode. As is illustrated in Fig. 1, QH–mode discharges have been run on DIII–D for periods of >4.0 s (>30 energy confinement times) with the duration limited only by machine hardware constraints. There are no known plasma physics limits to the duration of the QH–mode. In the past year, QH–mode operation has also been achieved in ASDEX Upgrade [19–21] and some QH–mode periods have been seen in discharges in JET [22] and JT60–U [23].

At present, QH–mode operation requires neutral beam injection in the direction opposite to the plasma current (counter injection) and some control of the plasma density (usually done with cryopumping); it is facilitated by having a 10 cm gap between the plasma and the vessel wall on the low field side [9,13,17]. QH–mode has been seen in single-null divertor discharges with the grad-B drift both towards and away from the X–point. As is discussed in this paper, a new achievement this year is QH–mode in magnetically balanced, double-null divertor discharges. QH–mode has been seen with input powers as low as 3 MW; maximum input power used to date is 13.6 MW. We have seen quiescent H–modes over the entire range of triangularity ($0.16 \le \text{delta} \le 0.82$) and safety factor q_{95} ($3.4 \le q_{95} \le 5.8$) explored to date. Most of our work has been done with plasma current in the range $1.0 \le I_p\ (\text{MA}) \le 2.0$ and toroidal field in the range $1.8 \le B_T\ (\text{T}) \le 2.1$. We also have quiescent H–mode examples at $I_p = 0.67$ MA and $B_T = 0.95$ T. Pedestal densities are in the range of $1\times10^{19}\text{m}^3$ to $6.5\times10^{19}\text{m}^3$. The radial profiles for the highest density QH–mode plasma run to date are shown in Fig. 2.

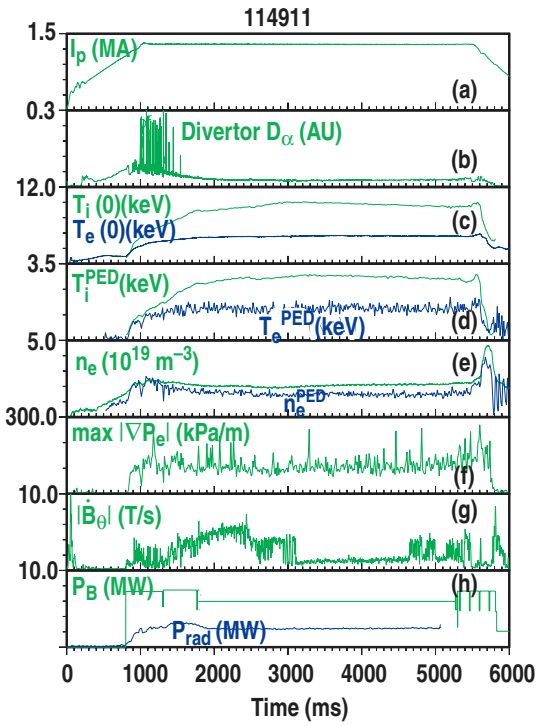

Fig. 1. Time history of one of the longest QH–mode discharges to date. (a) Plasma current, (b), divertor D_α signal, (c) central electron and ion temperatures, (d) pedestal electron and ion temperatures, (e) line averaged and pedestal electron density, (f) maximum electron pressure gradient in the edge pedestal, (g) rms amplitude of magnetic fluctuations showing the EHO, (h) injected neutral beam power and radiated power. As can be seen in (b), the quiescent phase in this shot lasts over 4 s even into the current ramp down. Notice that the maximum edge electron pressure gradient does not change significantly when the plasma goes from the ELMing to the quiescent phase around 1500 ms. There is also little variation in this gradient when the EHO switches from n=2 dominated to n=3 dominated at 3000 ms or when it switches back again to n=2 at 4650 ms.

A key feature of the QH–mode is the presence of an edge, electromagnetic oscillation dubbed the edge harmonic oscillation (EHO) [9]. The EHO enhances the particle transport through the edge without significantly increasing the thermal transport [9,13].

The goals of our QH–mode experiments in the 2003 campaign were to develop an improved physics understanding of the QH–mode operating regime and to broaden the QH–mode operating space through parameter scans suggested by MHD stability theory. A particular goal of the latter work was to develop robust techniques for operating QH–mode at higher densities.

This paper reports the results of the 2003 experiments with a particular focus on the edge radial electric field E_r. An edge E_r well is characteristic of all H–mode plasmas; the QH–mode well is significantly deeper than that in standard H–mode, reaching –100 kV/m in some cases as compared to the –20 kV/m to –30 kV/m seen in standard, ELMing H–mode. In particular, we have investigated the effect of edge fast ion orbit loss and edge triangularity on the E_r well.

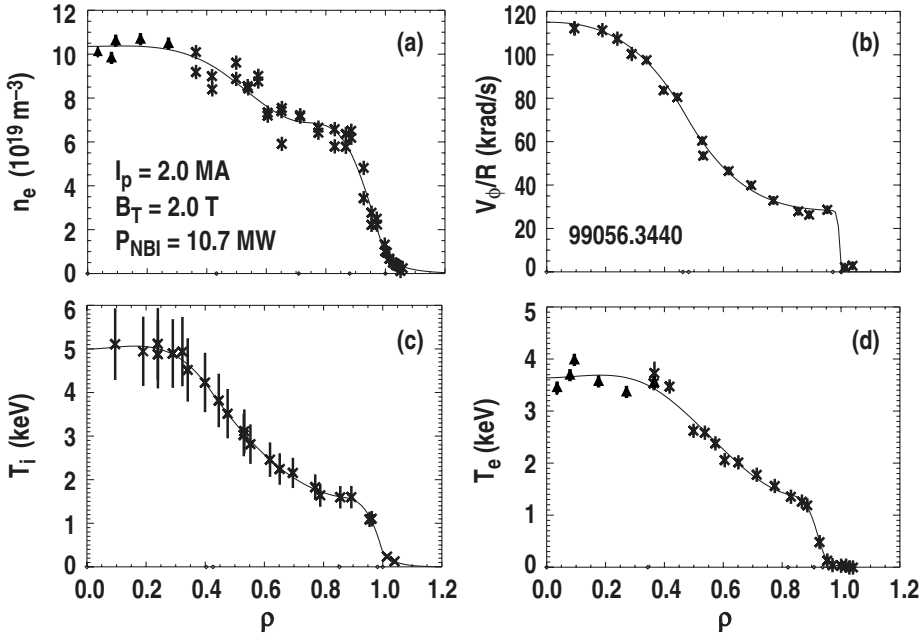

Fig. 2. Radial profiles of highest density QH–mode discharge run to date. (a) Electron density, (b) angular toroidal rotation speed, (c) ion temperature and (d) electron temperature.

2. EDGE SWEEP TECHNIQUE FOR IMPROVED E_R MEASUREMENTS

Previous work [13] has shown that the edge E_r well in QH–mode is both deep and quite narrow, with typical widths of about 1 cm. We determine E_r using our charge exchange spectroscopy system [24] to measure the temperature, density, poloidal and toroidal rotation of fully stripped carbon ions; E_r is then calculated from the radial force balance equation. Because the minimum radial spacing between the spectroscopic measurement points is 6 mm, it is quite possible to miss the bottom of the E_r well if the location of the plasma edge relative to the measurement points is not optimized. In order to be sure that we have measured the complete profile, we have swept the edge of the plasma across the measurement points to improve the spatial resolution. This technique is ideally suited for the QH–mode plasma since, as is shown in Fig. 1, the QH–mode edge can be essentially constant for several seconds. Typically, we move the edge 4–5 cm in about 500 ms during a steady-state portion of the discharge. The location of the high-field side of the plasma is kept constant during the sweep; accordingly, the plasma major and minor radii change by about 2 cm during the sweep.

As is shown in Figs. 3–5, this sweep technique provides extremely detailed edge profiles. Comparing the carbon density and temperature profiles in Fig. 3, we see that the scale length for both of these is about 1 cm. The rise in ion temperature in the scrapeoff layer (SOL) has been reported previously [16,17]; it may be due to the presence of fast ions in the SOL connected with the counter-injected orbits discussed in the next section. The structure of the edge carbon toroidal rotation (Fig. 4) with its negative region near the separatrix is characteristic of the QH–mode plasmas; co-injected discharges rarely exhibit this reversal of the toroidal rotation. The negative vertical velocity just inside the separatrix is typical of all H–modes in DIII–D. However, the detailed structure of the vertical velocity has only been seen in these sweep shots. A notable feature of the vertical velocity is the abrupt change in slope quite close to the separatrix. This is the only feature seen so far in a radial profile which shows a sharp change right at the separatrix.

The QH–mode edge electric field structure is shown in Fig. 5 for a typical QH–mode plasma. The width of the E_r well at the half-minimum point is about 1 cm. As can be seen in Fig. 5(b), both the $v \times B$ term and the pressure gradient term for carbon contribute significantly to the E_r structure. The width of the E_r well is actually close to the diameter of the gyro-orbit of a deuteron in the toroidal field at the radius of the well. Using the 2 keV ion temperature at the minimum of the E_r well seen Fig. 3(b), the gyroradius in the toroidal field for a deuteron is 0.6 cm. This suggests that some of the gyroradius scale effects discussed by Hazeltine et al. [25] may be important in the structure of the QH–mode E_r well.

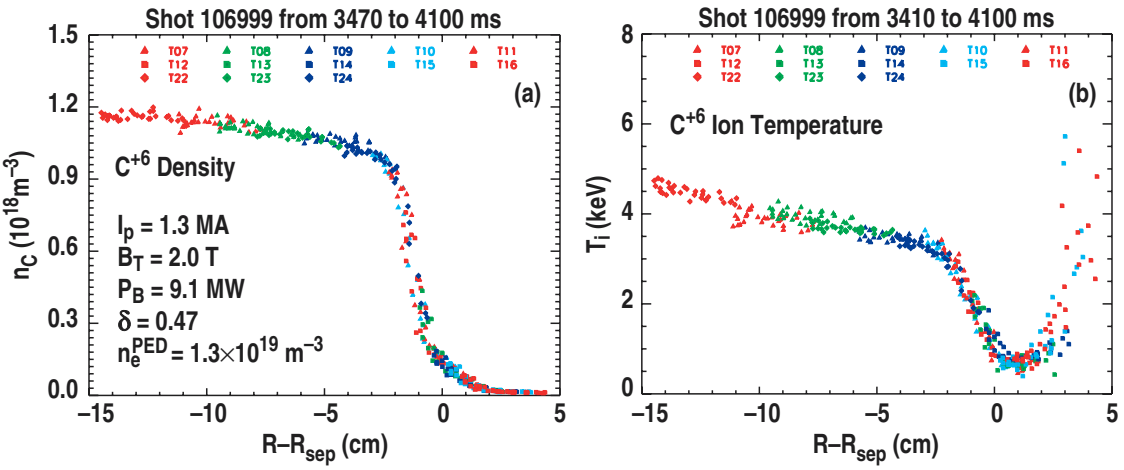

Fig. 3. (a) Density and (b) temperature of fully stripped carbon (C^{+6}) from charge exchange spectroscopy plotted as a function of distance from the separatrix at the low field midplane of the plasma. A sweep of the plasma edge is used to improve spatial resolution. The separatrix location at each measurement time is determine from MHD equilibrium analysis. Plasma conditions are 1.3 MA plasma current. 2.0 T toroidal field, 9.1 MW injected neutral beam power, 0.47 average triangularity, and $1.3\times10^{19}\,m^3$ pedestal electron density. The colors in the plot show the portion of the data that come from the different individual spatial measurement points. The agreement in the regions of overlap demonstrates that the edge plasma does not vary during the sweep.

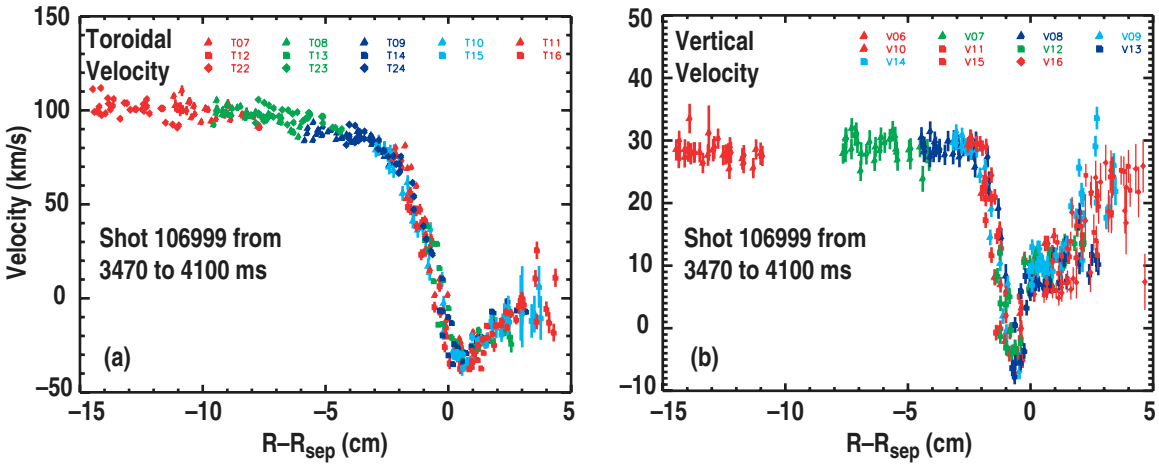

Fig. 4. Radial profile of velocity of fully stripped carbon (C^{+6}) as measured by (a) toroidally and (b) vertically viewing chords of the charge exchange spectroscopy system. Data are for the same shot as in Fig. 3. The colors in the plot show the portion of the data that come from the different individual spatial measurement points. The sign convention for the velocity has the toroidal rotation speed positive in the direction of the neutral beams while the vertical velocity is positive in the downwards direction on the low field side of the plasma. A positive toroidal velocity is in the opposite direction to the plasma current in these, counter-injected shots.

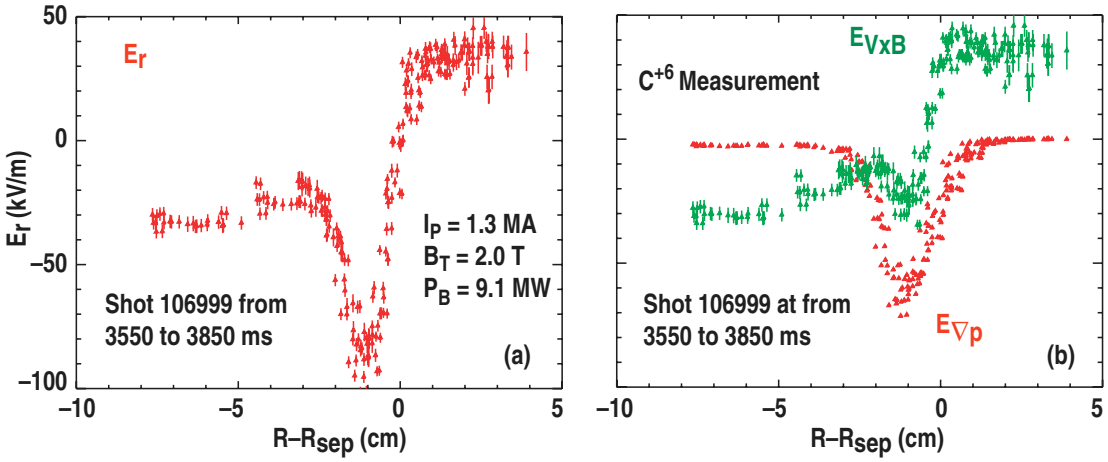

Fig. 5. (a) Edge profile of radial electric field determined from charge exchange spectroscopy using the edge sweep technique illustrated in Figs. 3 and 4. (b) Pressure gradient ($E_{\nabla P}$) and rotational ($E_{v\times B}$) contributions to the radial electric field for the (C^{+6}) radial force balance equation. Data are for the same shot as in Figs. 3 and 4.

The edge sweep technique has also been used to provide spatial cross calibration between various diagnostics viewing the plasma edge [26]. For example, the spatial location of the beam emission spectroscopy system was benchmarked against the charge exchange spectroscopy system by monitoring the same, Doppler-shifted D_α emission from the neutral beams with both systems. As is shown in Fig. 6, this allowed us to improve our knowledge of the spatial location of the density fluctuation associated with the edge harmonic oscillation. The peak of the fluctuations appears to be located about 2 cm inside the separatrix. Also shown in Fig. 6 is the first spatial derivative of the D_α emission from the beam. It peaks about 1 cm inside the separatrix. One early model of the EHO was based on the idea of a rigid oscillation of the plasma edge, similar to that produced by core tearing modes. However, such a model predicts that the peak in the density fluctuation should occur at the peak in the gradient of the D_α emission. Clearly, this is not seen in our data. The model of a rigid oscillation of the plasma edge is also inconsistent with the radial phase variation in the EHO density oscillation published previously [13]. Results from ASDEX–U [21] also indicate that the EHO is not a tearing mode.

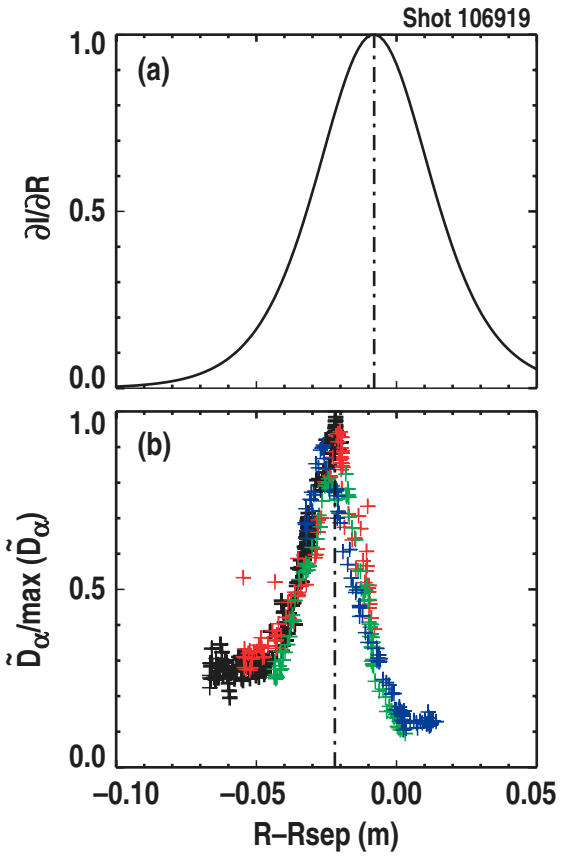

Fig. 6. Radial profiles of (a) normalized gradient of D_α intensity from the neutral beam and the (b) normalized amplitude of the density fluctuation associated with the dominant, n=2 component of the EHO. Each plot has the data normalized to the maximum of the data set. Both measurements come from beam emission spectroscopy data. The D_α intensity is the low frequency portion of the data while the density fluctuation information is the result of Fourier analysis of the higher frequency portion. The edge sweep is used to move the separatrix past the various viewpoints, thus building up the complete profile. Separatrix location is determined at each measurement time using MHD equilibrium analysis. In (b), the different colors show results from different viewchords. The good agreement demonstrates that the edge plasma does not vary during the sweep. Data are from shot 106919 which has the same basic plasma conditions as the shot used in Figs. 3–5.

3. EFFECTS OF EDGE FAST ION LOSS

A fundamental question for QH–mode is the role that counter injection plays. As is illustrated in Fig. 7, ion orbit loss calculations have shown that beam ions produced by ionization of fast neutrals injected by the so-called left sources results in prompt, first banana-orbit loss when the ionization occurs near the top of the H–mode edge pedestal. Ions from right beams, which are injected in a more perpendicular direction, are more deeply trapped and have narrower confined orbits. Most QH–mode experiments to date have favored the left sources because, at low densities, the shine-through loss of these beams is lower and because operational experience shows the QH–mode is easier to obtain with left sources [18]. Accordingly, a natural question is whether the direct orbit loss from the left sources is necessary to create and sustain the QH–mode.

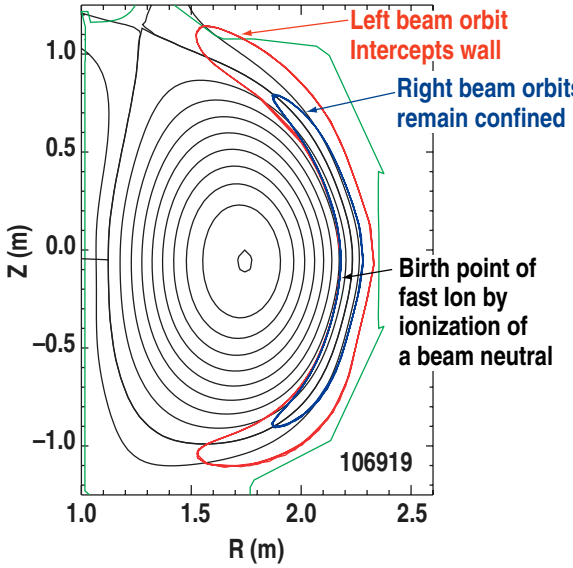

Fig. 7. Calculated banana orbits projected onto one poloidal plane. Results are shown for ions born at the top of the edge pedestal. As indicated, ions from the left sources are lost in one banana orbit while those from the right sources suffer no direct orbit loss. Plasma shape is from shot 106919; basic plasma conditions are the same as those in Fig. 3–6.

In order to test whether the left sources are essential for the QH–mode, we conducted experiments where we switched the beam injection from three left beam sources to three right beam sources at various times during the shot. As is shown in Figs. 8 and 9, all of these shots have the usual three left source combination in the low-density startup phase to prevent the early shine through losses from affecting the QH–mode portion of the experiment. As can be seen in Fig. 8, three right sources can sustain a QH–mode originally created with three left sources.

Figure 9 shows that switching to right sources in the ELMing phase delays the onset of the QH–mode substantially. Ultimately, however, the QH–mode still forms. Accordingly, we see that three right sources can both create and sustain the QH–mode. In other words, ion orbit loss from the left sources is not a necessary condition for the QH–mode.

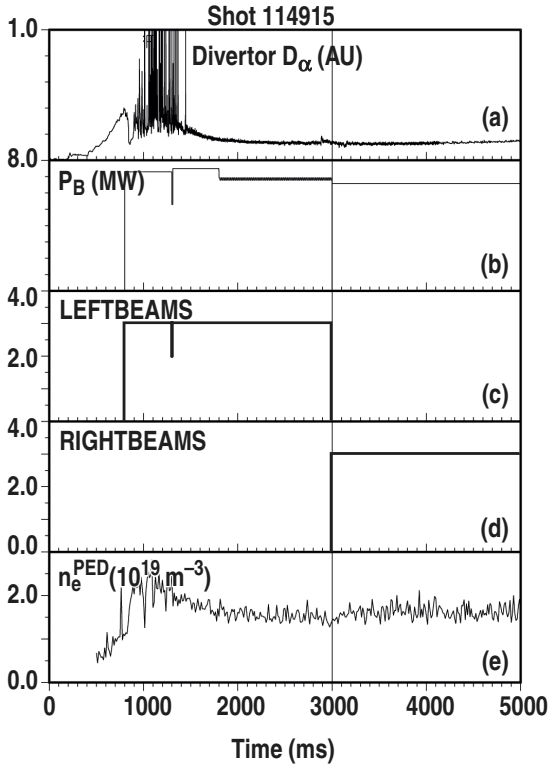

Fig. 8. Injection of three right neutral beam sources starting at 3000 ms (d) sustains a QH–mode plasma created using three left sources (c). Plasma shape is the same as that in Fig. 7. Plasma current is 1.3 MA and average triangularity is 0.47.

At present, we do not understand why the onset of the QH–mode is delayed with the right sources. One possibility is the higher pedestal density seen with right source injection; this is shown in Fig. 9. QH–mode is easier to form at lower densities. The higher pedestal density may simply be due to the increased fueling caused by the better confinement of the ions from the right sources.

We originally speculated that QH–modes favored left sources because of a difference in the edge E_r well related to the increased direct orbit loss. However, as is shown in Fig. 10, in the developed QH–mode, there is little difference in the E_r well structure or magnitude in left versus right source cases. There are some minor differences in the $v \times B$ and pressure gradient terms, but the E_r values are surprisingly similar. Since we need the edge sweep to determine the E_r structure accurately, we do not yet have information on the E_r time evolution during the formation phase of the QH–mode. It remains a possibility that the orbit loss from the left sources

is important at that time. However, in the developed QH–mode, it is clear that the direct orbit loss plays little role in the edge E_r structure.

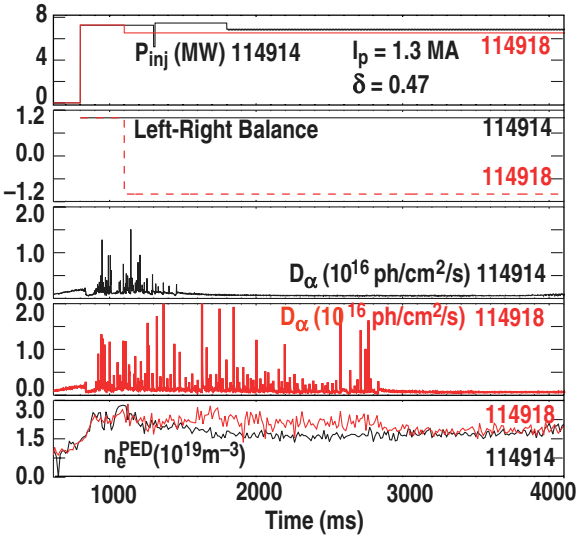

Fig. 9. Comparison of two shots, one with neutral beam injection from three left sources (Left-Right Balance = +1) and one where three right sources (Left-Right balance = –1) take over during the ELMing phase of the discharges. Both lead to a QH–mode; however, there is a significant delay in the QH–mode onset for the right source case. This delay is much longer than the usual shot-to-shot variation.

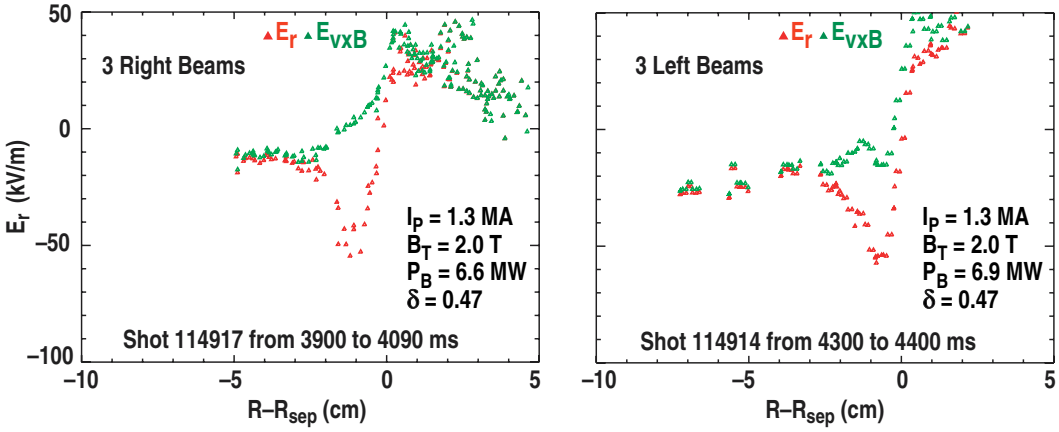

Fig. 10. Edge E_r profiles versus major radius relative to the separatrix for QH–mode plasmas with injection of three left and three right beam sources. There is little change in the E_r profiles. Basic plasma conditions are plasma current 1.3 MA, toroidal field 2.0 T and average triangularity 0.47.

Another interesting observation from the left to right source shots is the decrease in the frequency of the EHO which occurs when the plasma rotation slows down after the right sources take over. Because of the different angles relative to the toroidal direction, the right sources inject about 40% less angular momentum into the plasma than the left sources do. The EHO frequency drops by about the same factor as the toroidal rotation at the top of the edge pedestal.

4. EFFECT OF EDGE TRIANGULARITY

Because the QH–mode plasmas tend to operate at the low density end of the tokamak parameter space [13,17], a key issue for QH–mode studies is developing techniques to increase the density while still maintaining the quiescent state. Attempts to increase density by gas puffing or pellet injection almost uniformly lead to the return of ELMs. Early observations [9] suggest that increasing the edge triangularity can allow quiescent operation at significantly higher densities. The increased edge pressure seen in these previous shots [9] is qualitatively consistent with the predictions of MHD stability theory [27].

As is illustrated in Fig. 11, gradually increasing triangularity over a period of 500 ms in the QH–mode produces an increase in the pedestal density by a factor of about 2.5 with the plasma remaining quiescent for the rest of the shot. The triangularity change was effected by changing the plasma shape from an upward-biased, single-null discharge to a magnetically balanced double null; the shapes are shown in Fig. 12. The change in shape reduces the effectiveness of the upper cryopumps and allows the increase in density. However, the extra fueling alone is not the key since gas puffing or pellet injection typically quench the quiescent state.

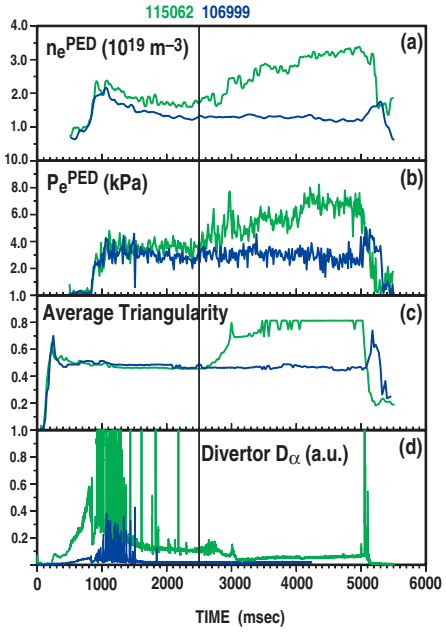

Fig. 11. Comparison of two QH–mode shots, one with triangularity increase after 2500 ms and another with constant triangularity. (a) pedestal electron density, (b) pedestal electron pressure, (c) average triangularity and (d) divertor D_α emission. In (d) the signal from the shot with the triangularity increase has been multiplied by a factor of 10 to separate the traces and show clearly the quiescent phase after 3000 ms. Both shots have 1.3 MA plasma current, 2.0 T toroidal field and 8.7 MW injected neutral beam power.

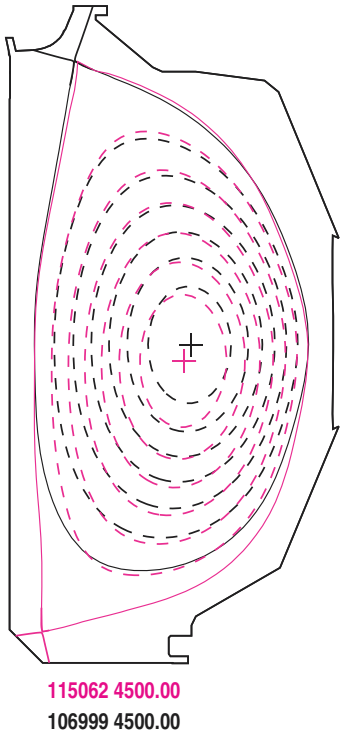

Fig. 12. Poloidal flux plots contrasting the shape of the upward biased single null and magnetically balanced double-null discharges shown in Fig. 11. The shot with the triangularity increase in Fig. 11 has the upper single-null shape until 2500 ms.

A somewhat higher pedestal pressure was achieved in later shots; this is illustrated in Fig. 13. As can be seen there, the pedestal electron and ion temperatures show little change from the reference shot as the triangularity and density increase. This suggests that the edge thermal conductivity depends weakly on density. Unfortunately, as sometimes happens during the edge sweep, the ELMs return transiently during that time in these later shots; hence, they do not demonstrate the long quiescent phase at higher density seen in Fig. 11.

The change in triangularity and/or pedestal density has a substantial effect on the edge E_r well as is seen in Fig. 14. The well is significantly shallower and somewhat broader than in the lower density, lower triangularity case shown in Fig. 5. This change in E_r is the largest that we have seen in our QH–mode studies.

In assessing the significance of the edge density values achieved in these shots, we run up against a fundamental conundrum of present-day tokamak physics. The best assessment is based on comparing pedestal density to those needed in next generation devices, such as ITER [1]. However, there are two contradictory ways of comparing the density. The nondimensional scaling approach [28] suggests comparing the values of the pedestal energy density β and collisionality ν^*. These are the two nondimensional parameters which involve the density; the third, the gyroradius normalized to machine size, only involves temperature and magnetic field. The divertor physics approach suggests comparing the density to the Greenwald density n_G [29]. Because of the explicit dependence of the Greenwald density on machine size, it is

impossible to operate a present day tokamak plasma simultaneously at the ITER values of β, ν^* and n_e/n_G.

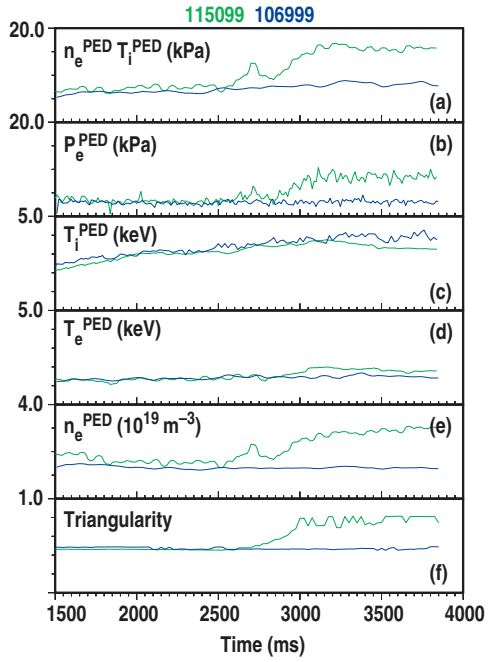

Fig. 13. Comparison of two QH–mode shots, one with and one without the triangularity increase. (a) estimate of pedestal ion pressure, (b) pedestal electron pressure, (c) pedestal ion temperature, (d) pedestal electron temperature, (e) pedestal electron density, and (f) average triangularity. Both shots are at 1.3 MA plasma current, 2.0 T toroidal field and 8.7 MW injected neutral beam power.

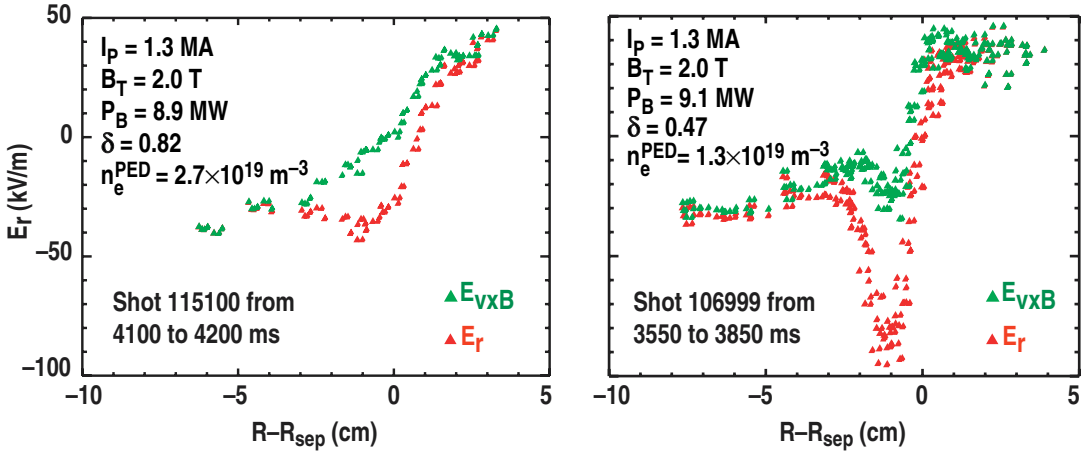

Fig. 14. Comparison of the E_r and C^{+6} $E_{v\times B}$ term for a moderate and a high triangularity shot. Notice the E_r well is shallower and somewhat broader for the case with triangularity $\delta = 0.82$.

As is illustrated in Fig. 15, the high triangularity shots achieve pedestal β and ν^* values which are quite close to the ITER values. The value of n_e^{PED}/n_G in the triangularity scan shots ranges from 0.1 at the lower triangularity to as high as 0.33 at the higher triangularities. Also

included in Fig. 15 are the results for the shot in Fig. 2. Accordingly, taken together, these shots demonstrate that QH–mode discharges can operate at ITER relevant values of pedestal β and ν*. They do not reach the ITER value of $n_e^{PED}/n_G = 0.7$ [30]; indeed, it is not clear that they need to in present devices to demonstrate relevance to future devices. The pedestal values influence the fusion gain by affecting the confinement and a nondimensional scaling is preferred in extrapolating confinement to next step devices [28].

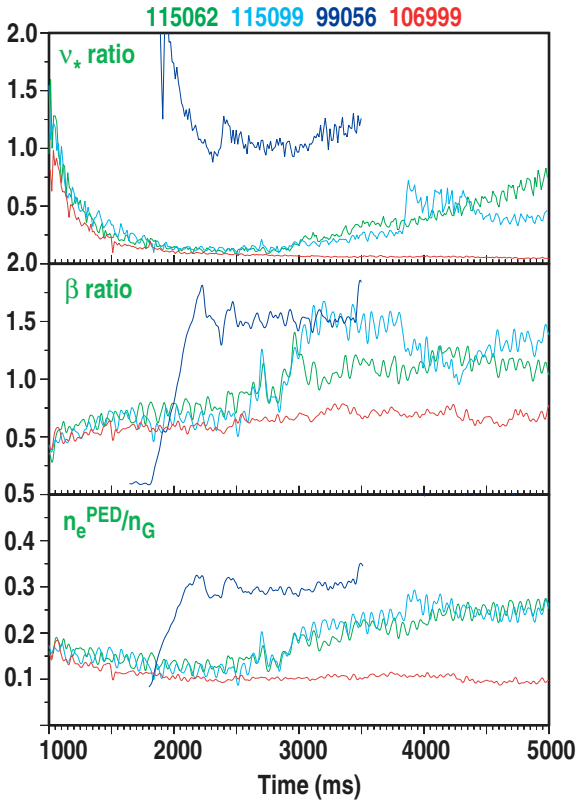

Fig. 15. Ratio of the DIII–D pedestal values of (a) ν^* and (b) β to the nominal ITER values. Also shown (c) is the ratio of the pedestal density to the Greenwald density. The ν^* and beta ratios are computed using the ITER values of edge safety factor q_{95} = 3, minor radius a = 2.0 m, pedestal electron density of 8.6×10^{19} m^3 and pedestal temperature of 3.9 keV. These values give a fusion gain of 10 according to confinement predictions using the GLF23 model [30].

One final interesting point about the high triangularity discharges is illustrated in Fig. 16. This shows the changes in the magnetic oscillations detected by the magnetic probes as the plasma changes to double null and the density rises. As the shape changes between 2500 ms and 3000 ms in this shot, the EHO switches toroidal mode number and its amplitude changes. Just after 3000 ms, the coherent EHO disappears and is replaced by broadband magnetic fluctuations. Since the plasma density reaches a steady state in these shots, we speculate that these broadband fluctuations are sufficient to provide the necessary particle transport. Although the coherent EHO

disappears completely in Fig. 16, some of the other high triangularity shots exhibit a mixture of the coherent EHO and the broadband fluctuations.

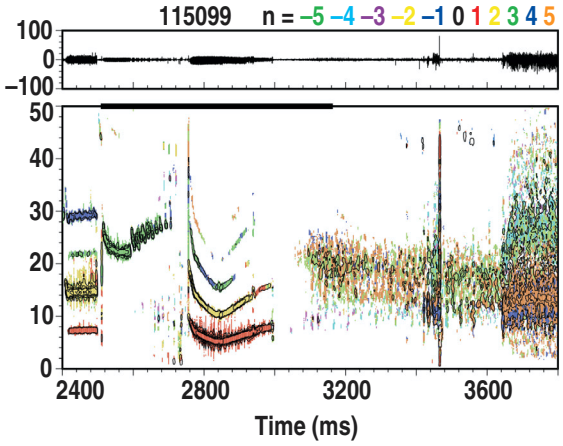

Fig. 16. Cross power spectra of two magnetic probes on DIII–D during the triangularity increase and higher density phases of the shot shown in Fig. 13. Notice that the coherent EHO is replaced by a broadband structure at the higher triangularity.

5. CONCLUSIONS

The steady-state nature of the QH–mode edge allows us to obtain unprecedented spatial resolution of the edge ion profiles and E_r by sweeping the edge plasma past the view points of the charge exchange spectroscopy system. Because the E_r well in QH–mode is so deep (about –100 kV/m) and so narrow (about 1 cm), this technique is essential for determining the true depth and shape of the well. The edge sweeps have also provided important spatial cross calibration with the beam emission spectroscopy system, allowing us to determine that the peak of the density fluctuation associated with the EHO is about 2 cm inside the separatrix and demonstrating that the EHO is not just a rigid oscillation of the plasma edge.

Investigations comparing the effects of left versus right neutral beam sources have shown that direct ion orbit loss is not necessary to create or sustain the QH–mode. However, the QH–mode is obtained more easily with left sources. In the fully developed QH–mode, the structure of the E_r well at the plasma edge is not affected by altering the direct ion orbit loss.

We have now demonstrated QH–mode operation in magnetically balanced double-null discharges. Utilizing the higher triangularity in the double-null shape, we have increased the pedestal density by a factor of about 2.5 and the overall pedestal pressure by a factor of about two while still maintaining quiescent operation. Pedestal β and ν^* values matching the values desired for ITER have been demonstrated. In these plasmas, the edge E_r well becomes significantly shallower and broader.

REFERENCES

[1] ITER Physics Basis Document, Nucl. Fusion **39** (1999) 2137.
[2] T.S. Taylor, H. St. John, A.D. Turnbull, Y.R. Lin-Liu, K.H. Burrell, V. Chan, M.S. Chu, J.R. Ferron, L.L. Lao, R.J. La Haye, E.A. Lazarus, R.L. Miller, P.A. Politzer, D.P. Schissel, E.J. Strait, Plasma Physics and Controlled Fusion Research **36** (1994) B229.
[3] T.S. Taylor, Plasma Phys. Control. Fusion **39** (1997) B47.
[4] A.W. Leonard, A. Hermann, K. Itami, J. Lingertat, A. Loarte, T.H. Osborne, W. Suttrop, J. Nucl. Mater. **266–269** (1999) 100.
[5] A.W. Leonard, T.H. Osborne, M.E. Fenstermacher, R.J. Groebner, M. Groth, C.J. Lasnier, M.A. Mahdavi, T.W. Petrie, P.B. Snyder, J.G. Watkins and L. Zeng, Phys. Plasmas **10** (2003) 1765.
[6] A.C.C. Sips, "Control of Transport Barriers," submitted to Plasma Phys. Control. Fusion
[7] K.H. Burrell, Rev. Sci. Instrum. **72** (2001) 906.
[8] K.H. Burrell, C.M. Greenfield, W.P. West, M.R. Wade, C. Rost, Bull. Am. Phys. Soc. **44** (1999) 127.
[9] K.H. Burrell, M.E. Austin, D.P. Brennan, J.C. DeBoo, E.J. Doyle, C. Fenzi, C. Fuchs, P. Gohil, C.M. Greenfield, R.J. Groebner, L.L. Lao, T.C. Luce, M.A. Makowski, G.R. McKee, R.A. Moyer, C.C. Petty, M. Porkolab, C.L. Rettig, T.L. Rhodes, J.C. Rost, B.W. Stallard, E.J. Strait, E.J. Synakowski, M.R. Wade, J.G. Watkins, and W.P. West Phys. Plasmas **8** (2001) 2153.
[10] R.J. Groebner, D.R. Baker, K.H. Burrell, T.N. Carlstrom, J.R. Ferron, P.Gohil, L.L. Lao, D.M. Thomas, T.H. Osborne, and W.P. West, Nucl. Fusion **41** (2001) 1789.
[11] C.M. Greenfield, K.H. Burrell, J.C. DeBoo, E.J. Doyle, B.W. Stallard, E.J. Synakowski, C. Fenzi, P. Gohil, R.J. Groebner, L.L. Lao, M.A. Makowski, G.R. McKee, R.A. Moyer, C.L. Rettig, T.L. Rhodes, R.I. Pinsker, G.M. Staebler, W.P. West, and the DIII–D Team, Phys. Rev. Lett. **86** (2001) 4544.
[12] E.J. Doyle, L.R. Baylor, K.H. Burrell, T.A. Casper, J.C. DeBoo, D.R. Ernst, A.M. Garofalo, et al., Plasma Phys. Control. Fusion **43** (2001) 95.
[13] K.H. Burrell, M.E. Austin, D.P. Brennan, J.C. DeBoo, E.J. Doyle P. Gohil et al., Plasma Phys. Control. Fusion **44** (2002) A253.
[14] C.M. Greenfield, K.H. Burrell, E.J. Doyle, R.J. Groebner, W.P. West, T.A. Casper, J.C. DeBoo, et al., Plasma Phys. Control. Fusion **44** (2002) A123.
[15] W.P. West, M.R. Wade, C.M. Greenfield, E.J. Doyle, K.H. Burrell, N.H. Brooks, P. Gohil, R.J. Groebner, G.L. Jackson, J.E. Kinsey, C.J. Lasnier, J. Mandrekas, G.R. McKee, T.L. Rhodes, G.M. Staebler, G. Wang, J.G. Watkins, and L. Zeng, Phys. Plasmas **9** (2002) 1970.

[16] C.J. Lasnier, K.H. Burrell, J.S. deGrassie, A.W. Leonard, R.A. Moyer, G.D. Porter, J.G. Watson and DIII–D Team, J. Nucl. Mater. **313–316** (2003) 904.

[17] E.J. Doyle, T.A. Casper, K.H. Burrell, C.M. Greenfield, W.P. West, et al., "Core and edge aspects of quiescent double barrier operation on DIII–D, with relevance to critical ITB physics issues," submitted to Nucl. Fusion.

[18] W.P. West, K.H. Burrell, E.J. Doyle, C.M. Greenfield, C.J. Lasnier, P.B. Snyder and L. Zeng, Proc. 30th EPS Conf. on Control. Fusion and Plasma Physics, St. Petersburg, 2003 (European Physical Society, Geneva 2003) CD-ROM, 27B.

[19] W. Suttrop, M. Maraschek, G.D. Conway, H.-U. Fahrbach, G. Haas, L.D. Horton, T. Kurki-Suonio, C.J. Lasnier, A.W. Leonard, C.F. Maggi, H. Meister, A. Mück, R. Neu, I. Nunes, Th. Pütterich, M. Reich, A.C.C. Sips, and ASDEX Upgrade Team, Plasma Phys. Control. Fusion **45** (2003) 1399.

[20] W. Suttrop, M. Maraschek, G.D. Conway, H.-U. Fahrbach, L. Fattorini, G. Haas, L.D. Horton, S. Klose, T. Kurki-Suonio, C.F. Maggi, P.J. McCarthy, H. Meister, A. Mück, R. Neu, I. Nunes, Th. Pütterich, M. Reich, A.C.C. Sips, ASDEX Upgrade Team, Proc. 30th EPS Conf. on Control. Fusion and Plasma Physics, St. Petersburg, 2003 (European Physical Society, Geneva 2003) CD-ROM, 27B.

[21] W. Suttrop, M. Maraschek, G.D. Conway, H.-U. Fahrback, G. Haas, L.D. Horton, T. Kurki-Suonio, C.F. Maggi, H. Meister, A. Muck, R. Neu, I. Nunes, Th. P. Utterich, M. Reich, A.C.C. Sips and the ASDEX Upgrade Team, "Stationary ELM-free H–mode in ASDEX Upgrade," submitted to Plasma Phys. Control. Fusion.

[22] W. Suttrop, private communication (2003).

[23] Y. Sakamoto, H. Shirai, T. Fujita, S. Ide, T. Takizuka, N. Oyama, Y. Kamada, "Impact of toroidal rotation on ELM behavior in H–mode and ITB plasmas on JT–60U," submitted to Plasma Physics Control. Fusion.

[24] K.H. Burrell, D.H. Kaplan, P. Gohil, D.G. Nilson, R.J. Groebner, D.M. Thomas, Rev. Sci. Instrum. **72** (2001) 1028.

[25] R.D. Hazeltine, H. Xiao, P.M. Valanju, Phys. Fluids B **5** (1993) 4011.

[26] W.M. Solomon, K.H. Burrell, P. Gohil, R. Groebner, D. Kaplan, and R. Nazikian, to be published in Rev. Sci. Instrum.

[27] P.B. Snyder, H.R. Wilson, Plasma Physics Control. Fusion **45** (2003) 1671.

[28] C.C. Petty, T.C. Luce, J.G. Cordey, D.C. McDonald, "Similarity ν^* rather than n/n_{limit} should be kept fixed in H–mode energy confinement," submitted to Plasma Physics Control. Fusion.

[29] M. Greenwald, R.L. Boivin, F. Bombarda, et al., Nucl. Fusion **37** (1997) 793.

[30] J.E. Kinsey, G.M. Staebler, and R.E. Waltz. "Burning Plasma Confinement Projections and Renormalization of the GLF23 Drift-wave Transport Model," to be published in Fus. Sci. and Tech. (2003).

ACKNOWLEDGEMENT

This work supported by the U.S. Department of Energy under Contract Nos. DE-AC03-99ER54463, W-7405-ENG-48, DE-AC02-76CH03073, DE-AC05-00OR22725, DE-AC04-94AL85000, and Grant Nos. DE-FG03-01ER54615, DE-FG03-97ER54415, DE-FG03-96ER54373.